

Photoinduced molecular orientation of catalytic-like chiral azo-schiff base complexes in PMMA or laccase matrices

Chigusa Kominato¹, Takashiro Akitsu^{1,*}

¹Department of Chemistry, Faculty of Science, Tokyo University of Science, 1-3 Kagurazaka, Shinjuku-ku, Tokyo 162-8601, Japan

*corresponding author e-mail address: akitsu@rs.kagu.tus.ac.jp

ABSTRACT

Due to the anisotropic environment provided by their peptide ligands and the molecular orientation of their active sites, metalloproteins exhibit biological activities such as directional electron transfer and selective redox reactions. Recently, we investigated the polarized ultraviolet (UV)-light-induced molecular orientation of chiral Schiff base complexes containing azo-groups in organic/inorganic hybrid materials. The Weigert effect results in a parallel orientation of the solutes. This behavior was observed using polarized spectroscopy as an increase in the optical dichroism and confirmed with time-dependent density functional theory (TD-DFT) calculations. Herein are described new organic/inorganic hybrid systems comprising azo-containing chiral Schiff base nickel(II), copper(II), and zinc(II) complexes, and polymethylmethacrylate (PMMA) or the copper protein laccase, which catalyzes the four electron reduction of oxygen to water along with the oxidation of the substrate.

Keywords: *Azobenzene, Weigert effect, polarized spectroscopy, laccase, chiral Schiff base complexes.*

1. INTRODUCTION

Organic/inorganic hybrid materials such as photochromic dyes (*e.g.*, azobenzene (AZ) and inorganic complexes have been widely studied as promising candidates for optical and/or magnetic data recording devices. One of the advantages of organic/inorganic hybrid materials is the ability to design multifunctional materials with supramolecular structures, for example metal complexes incorporating azo-ligands with large dichroic ratios [1,2]. Recently, organic/inorganic hybrid materials comprising photochromic organic compounds and magnetic inorganic compounds were reported to exhibit reversible photomagnetic switching [3-8]. We have also employed inorganic complexes with various functionalities, including those whose fluorescence intensity depends on intermolecular interactions [9, 10], those capable of molecular recognition of chirality [11-13], and those that exhibit molecular-based magnetism [14-17].

Metalloproteins may be regarded as metal complexes with remarkably intricate peptide ligands. In particular, phenolate, thiolate, oxo, sulfido, and *N*-heterocyclic chelates in metalloproteins exhibit extremely intense low energy charge-transfer (CT) absorption bands, which reflect highly covalent ligand-metal bonds. These features are attributed to the electronic structures of the active sites and are affected by the coordination geometries of the metal sites and the spatial orientation of the metal-ligand coordination bonds. Consequently, such stereochemical features can be influenced by the protein matrix [18]. Spectroscopy plays a major role in understanding the active sites of metalloproteins. Copper active sites in metalloproteins often exhibit unique spectral features different from small-molecule copper complexes. The unique electronic features of these active sites are derived from their unusual geometry, and hence, electronic structures can be imposed on the metal ions through

intermolecular interactions with the surrounding protein biopolymers [19]. This behavior is notably similar to that observed in organic/inorganic hybrid materials.

The structural characterization of biomaterials is challenging because they are typically too large for nuclear magnetic resonance (NMR) or high-resolution mass spectrometry and their irregular structures are unsuitable for X-ray crystallography. Structural characterization and kinetic analysis of such systems thus must be achieved by collecting complementary data using different techniques. For example, fluorescence polarization was first applied in biochemistry nearly six decades ago, when Gregorio Weber described his studies on bovine serum albumin and ovalbumin conjugated with 1-dimethylaminonaphthalene-5-sulfonyl chloride (dansyl chloride) [20,21]. While polarized spectroscopic methods became increasingly popular during the decades following Weber's work, in the past few decades, the increase in the number and diversity of fluorescence polarization studies has been astonishing. This method is now extremely widespread in clinical and biomedical fields [22].

Linear dichroism (LD), a polarized spectroscopic technique applied to oriented molecular systems, can also be used to provide useful data on biomaterials. In particular, LD can provide information about the relative orientations of subunits of proteins and the orientations of whole biomaterials with respect to an orientation axis [23]. Electronic circular dichroism (ECD) spectra of flexible molecules reveal the contributions of all conformers populated at the working temperature. In particular, the ECD spectrum of a chiral substrate depends on its stereochemistry in terms of both its absolute configuration as reflected in the sign of the spectrum and its molecular conformation, which dictates the

overall spectral shape (possibly including the sign) in a very sensitive manner [24].

We have found that photo-tuning the optical anisotropy of **AZ** can provide valuable information [31,32]. Specifically, we have focused on the polarized ultraviolet (UV)-light-induced alignment caused by the selective photoisomerization and molecular reorientation of **AZ** (the Weigert effect) [25, 26], rather than the conventional *cis-trans* photoisomerization of **AZ**. For related organic/inorganic hybrid materials with photo-induced dichroism, the electric-transition dipole moment should be considered to gain a greater understanding and a clearer interpretation of the angular dependence of the absorbance of the polarized spectra. Therefore, to discuss the degree of the molecular orientation of components, polarized spectra have been observed for organic/inorganic hybrid materials [4-6, 33-35].

Recently we investigated the linearly polarized UV light-induced molecular orientation of chiral Schiff base nickel(II), copper(II), and zinc(II) complexes in organic/inorganic hybrid materials containing **AZ** in a polymethylmethacrylate (PMMA) matrix [33-36]. The Weigert effect resulted in the parallel orientation of the solutes (chiral complexes and **AZ**), which was observed using polarized spectroscopy, and this optical dichroism was discussed using time-dependent density functional theory (TD-DFT) calculations.

2. EXPERIMENTAL SECTION

2.1. General procedure.

Chemicals of the highest commercial grade available (solvents from Kanto Chemical, organic compounds from Tokyo Chemical Industry, and metal sources and laccase from Wako Pure Chemical Industries, Ltd.) were used as received without further purification. The compound 4-phenyldiazenylsalicylaldehyde was prepared in a manner similar to that for analogous compounds [38, 39].

2.2. Preparation of **1**.

To a solution of 4-phenyldiazenylsalicylaldehyde (0.2261 g, 1.00 mmol) dissolved in methanol (50 mL), *R*-(*-*)-2-phenylglycianol (0.1372 g, 1.00 mmol) was added dropwise, and the mixture was stirred at 313 K for 2 h to give an orange solution of the ligand. Nickel(II) acetate tetrahydrate (0.1244 g, 0.500 mmol) was then added to this solution. After stirring for 2 h, the crude compound was filtered to give a green precipitate. Unfortunately, single crystals suitable for X-ray analysis could not be obtained. Yield 0.1800 g (48.17%). Anal. Found: C, 66.1%; H, 5.25%; N, 10.8%. Calc. for $C_{42}H_{36}NiN_6O_4$: C, 66.3%; H, 5.17%; N, 10.8%. IR (Nujol (cm^{-1})): 722 m, 1110w, 1307w, 1377s, 1463s, 1524w(N=N), 1592w, 1631w(C=N), 2727w, 2854s, 2925s. UV-vis (diffuse reflectance): 10400, 20700, 28100, 37900 cm^{-1} .

2.3. Preparation of **2**.

To a solution of 4-phenyldiazenylsalicylaldehyde (0.2261 g, 1.00 mmol) dissolved in methanol (50 mL), *R*-(*-*)-2-phenylglycianol (0.1372 g, 1.00 mmol) was added dropwise, and the mixture was stirred at 313 K for 2 h to give an orange solution of the ligand. Copper(II) acetate monohydrate (0.0998 g, 0.500 mmol) was then added to the solution. After stirring for 2 h, the crude compound was filtered to give a brown precipitate. Unfortunately, single crystals suitable for X-ray analysis could not

be obtained. Yield 0.1368 g (77.95 %). Anal. Found: C, 65.7%; H, 5.40%; N, 10.8%. Calc. for $C_{42}H_{36}CuN_6O_4$: C, 65.8%; H, 5.14%; N, 10.7%. IR (Nujol (cm^{-1})): 723w, 838w, 1112w, 1307w, 1378 m, 1465s, 1525w(N=N), 1607w, 1630 m(C=N), 2724w, 2853s, 2925s. UV-vis (diffuse reflectance): 16000, 21600, 37900 cm^{-1} .

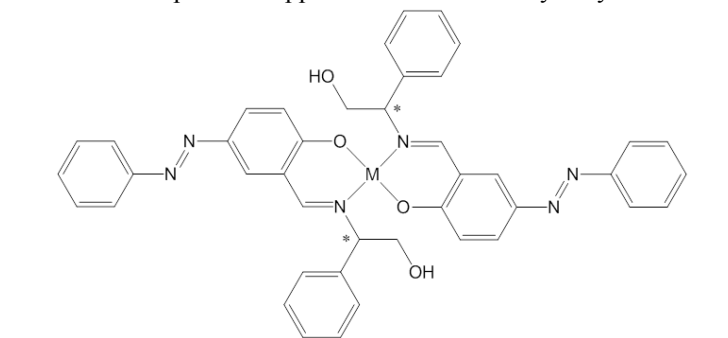


Figure 1. Structure of chiral Schiff base Ni(**1**), Cu(**2**), and Zn(**3**) complexes.

be obtained. Yield 0.3283 g (91.09%). Anal. Found: C, 64.9%; H, 4.94%; N, 10.4%. Calc. for $C_{42}H_{36}ZnN_6O_4$: C, 65.6%; H, 5.13%; N, 10.7%. IR (Nujol (cm^{-1})): 722w, 838w, 1112w, 1307w, 1377 m, 1464s, 1518w(N=N), 1614w, 1630w(C=N), 2727w, 2854s, 2923s. UV-vis (diffuse reflectance): 21600, 37900 cm^{-1} .

2.4. Preparation of **3**.

To a solution of 4-phenyldiazenylsalicylaldehyde (0.2261 g, 1.00 mmol) dissolved in methanol (50 mL), *R*-(*-*)-2-phenylglycianol (0.1372 g, 1.00 mmol) was added dropwise, and the mixture was stirred at 313 K for 2 h to give orange solution of ligand. Zinc(II) acetate tetrahydrate (0.1098 g, 0.500 mmol) was then added to the solution. After stirring for 2 h, the crude compound was filtered to give a yellow precipitate. Unfortunately, single crystals suitable for X-ray analysis could not be obtained. Yield 0.3283 g (91.09%). Anal. Found: C, 64.9%; H, 4.94%; N, 10.4%. Calc. for $C_{42}H_{36}ZnN_6O_4$: C, 65.6%; H, 5.13%; N, 10.7%. IR (Nujol (cm^{-1})): 722w, 838w, 1112w, 1307w, 1377 m, 1464s, 1518w(N=N), 1614w, 1630w(C=N), 2727w, 2854s, 2923s. UV-vis (diffuse reflectance): 21600, 37900 cm^{-1} .

2.5. Preparation of hybrid materials **1+PMMA**, **2+PMMA**, and **3+PMMA**.

An acetone solution (0.5 mL) of **1**, **2**, or **3** (0.0019 g in 5 mL acetone) and an acetone solution (2 mL) of PMMA (10%) were cast onto a slide glass and dried overnight at room temperature to give rise to a PMMA film of the hybrid material **1+PMMA**, **2+PMMA** or **3+PMMA**.

2.6. Preparation of hybrid materials **1+laccase**, **2+laccase**, and **3+laccase**.

An acetone solution (0.5 mL) of **1**, **2**, or **3** (0.0019 g in 5 mL acetone) and laccase (0.0152 g in 2 mL Tris (*tris*(hydroxymethyl)aminomethane) buffer) were mixed and

dropped onto a PMMA film and dried for 2 days at room temperature to give rise to the hybrid materials **1+laccase**, **2+laccase**, and **3+laccase**.

2.7. Physical measurements.

Elemental analyses (C, H, N) were performed using a Perkin-Elmer2400II CHNS/O analyzer at the Tokyo University of Science. Infraredspectra (IR) spectra were recorded as Nujolmulls on a JASCO FT-IR 4200 plusspectrophotometerequipped with a polarizer over a range of 4000–400 cm^{-1} at 298 K. Electronic spectra were obtained on a JASCO V-650 or V-570UV/VIS/NIR spectrophotometer equipped with a polarizer over the range of 800–220 nm at 298 K. Circular dichroism (CD) spectra were

3. RESULTS SECTION

3.1. Electronic and CD spectra.

Figure 2 shows a comparison of the simulated (calculated) and experimental electronic and CD spectra to confirm reliable band assignments. In the experimental electronic spectra, d–d bands appeared at 635 and 603 nm for **1** and **2**, respectively. In addition, π – π^* bands appeared at 376, 382, and 360 nm, and n– π^* bands appeared at 245, 254, and 275 nm for **1**, **2**, and **3**, respectively. In the experimental CD spectra, π – π^* bands appeared at 396, 387, and 391 nm, while n– π^* bands appeared at 259, 266, and 258 nm for **1**, **2**, and **3**, respectively. On the other hand, in the simulated spectra, d–d bands appeared at 749 and 577 nm and the transition electric dipole moments were determined to be (–0.2417, 0.0527, –0.0495) and (0.8836, –0.1533, 0.0281) with oscillator strengths of 0.0026 and 0.0424 for **1** and **2**, respectively. According to previous studies on related compounds, the optimized structures and assignments of the transitions for **1**, **2**, and **3** are reasonable [32, 35].

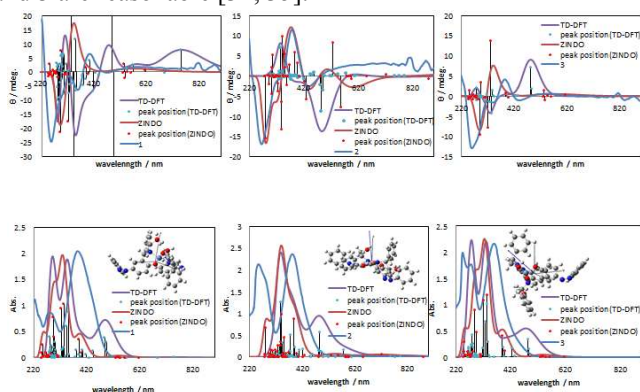


Figure 2. Simulated ZINDO (red) and TD-DFT (purple) and experimental (blue) electronic spectra (bottom) and CD spectra (top) for **1** (left), **2** (middle), and **3** (right) with optimized structures.

Selected predominant peaks were assigned to transitions between molecular orbitals as follows: for **1**, 749 nm (d–d band)(HOMO (190) to LUMO (191)), 351 nm (π – π^* band)(HOMO-2 (188) to LUMO+1 (191)) and 280nm (HOMO-7 (183) to LUMO+2 (193)); for **2**, 791 nm (d–d band)(HOMO-3 (189 β) to LUMO (191 β)), 486 nm (π – π^* band)(HOMO-1 (190 β) to LUMO+6 (194 β)) and 336 nm (n– π^* band)(HOMO-8 (187 α) to LUMO+1 (192 α)); for **3**, 334 nm (π – π^* band)(HOMO-2 (185) to LUMO+2 (190)) and 279 nm (n– π^* band)(HOMO-9 (178) to LUMO (188)).The magnitude of the dipole moments obtained from the optimized structures were 2.2949 Debye (–2.0160,

recorded on a JASCO J-820 spectrophotometer at 298 K. Photo-irradiation was performed using a 200–350 nm D₂ light source (with a visible cut filter) and a 350–800-nm Xe light source (with a UV cut filter) using a polarizer.

2.8. Computational methods.

All calculations were performed using the Gaussian 09W software Revision A.02 (Gaussian, Inc.) [40].The gas phase geometry optimizations were performed using TD-DFT at the B3LYP level. The vertical excitation energies were calculated using the Lan2dz and 6–31+G(d) basis sets for Ni, Cu, and Zn and H, C, N, and O, respectively, assuming a singlet ground-state geometry.

0.6129, 0.9092) for **1**, 6.2179 Debye (–1.0971, 0.0872, 6.1197) for **2**, and 6.3329 Debye (–0.5829, –4.5736, 4.3414) for **3**.

3.2. Polarized absorption spectra of PMMA systems after linearly polarized UV light irradiation.

After polarized UV light irradiation, the intensity (absorbance as measured) of selected characteristic peaks was determined for the polarized absorption spectra of the PMMA systems containing the chiral Schiff base complexes. The spectra shown in Figures 3–5 were obtained using a polarizer aligned at 0° before (0 min) and after polarized UV light irradiation for 10 min. Spectra were also obtained at every 5° from 0° to 90° both before and after polarized UV light irradiation for 0.5, 1, 3, 5, and 10 min.

Figure 3 shows the polarized absorption spectra and circular diagrams (angular dependence of the absorbance) for the π – π^* band at 318 nm and n– π^* band at 440 nm for **AZ** and the d–d band at 612 nm for **1** in **1+PMMA**[15, 17, 30]. The initial change in the π – π^* band is attributed to the *cis-trans* photoisomerization of **AZ**. The circular diagrams suggest that reorientation of **AZ** influenced the relatively high optical anisotropy observed for the π – π^* and n– π^* bands. Specifically, polarized UV light irradiation induced optical anisotropy along with a significant decrease in the intensity of the π – π^* band.

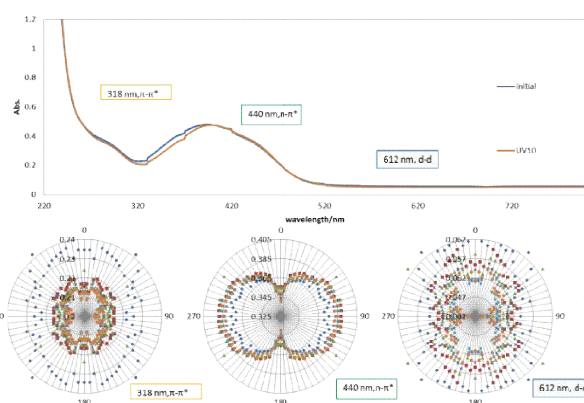


Figure 3.(Top) Polarized absorption spectra for **1+PMMA** at 0° showing predominant peaks before and after UV light irradiation for 10 min. (Bottom) Circular diagrams of the angular dependence of the absorbance of the predominant peaks in the polarized absorption spectra for **1+PMMA** after UV light irradiation for 0 (blue), 0.5 (red), 1 (green), 3 (violet), 5 (light blue), and 10 (orange) min.

Figure 4 shows the polarized absorption spectra and circular diagrams for the π – π^* band at 318 nm and the n– π^* band at 440 nm of **AZ** and the d–d band at 682 nm for **2** in

2+PMMA[16, 17, 41]. An initial change in the π - π^* band was also observed because of the *cis-trans* photoisomerization of AZ [36].

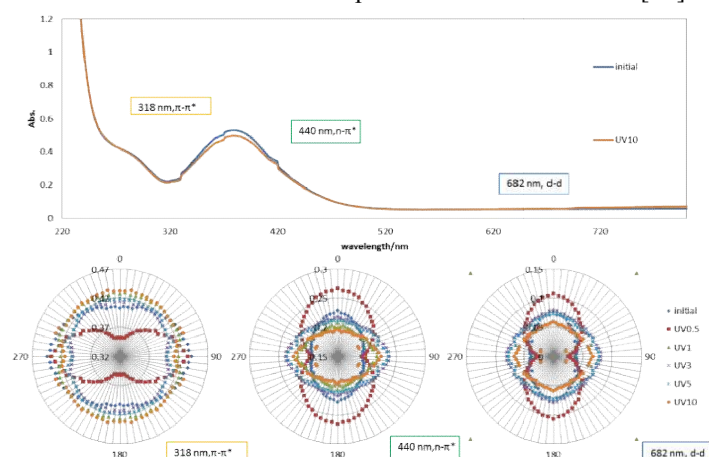


Figure 4. (Top) Polarized absorption spectra for 2+PMMA at 0° showing predominant peaks before and after UV light irradiation for 10 min. (Bottom) Circular diagrams of the angular dependence of absorbance of the predominant peaks in the polarized absorption spectra for 2+PMMA after UV light irradiation for 0 (blue), 0.5 (red), 1 (green), 3 (violet), 5 (light blue), and 10 (orange) min.

Figure 5 shows the polarized absorption spectra and circular diagrams for the π - π^* band at 318 nm and n - π^* band at 440 nm for AZ in 3+PMMA.

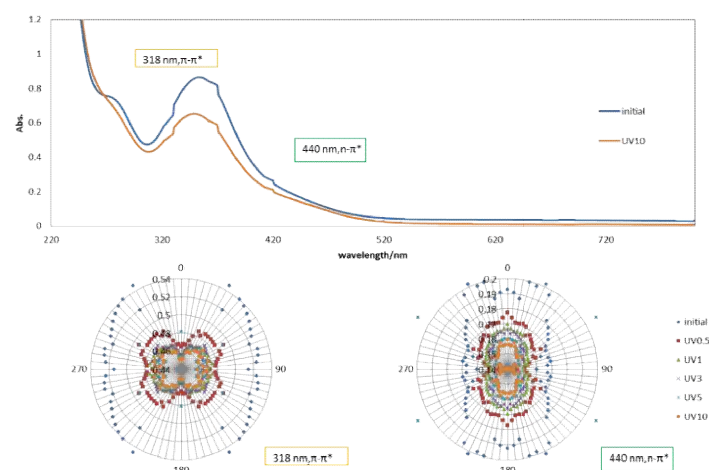


Figure 5: (Top) Polarized absorption spectra for 3+PMMA at 0° showing predominant peaks before and after UV light irradiation for 10 min. (Bottom) Circular diagrams of the angular dependence of the absorbance of the predominant peaks in the polarized absorption spectra for 3+PMMA after UV light irradiation for 0 (blue), 0.5 (red), 1 (green), 3 (violet), 5 (light blue), and 10 (orange) min.

3.3. Polarized absorption spectra of laccase systems after polarized UV light irradiation.

Figure 6 shows the polarized absorption spectra and circular diagrams for the π - π^* band at 318 nm and the n - π^* band at 440 nm of AZ and the d-d band at 638 nm of 1 in 1+laccase. Here again, the initial change in the π - π^* band was attributed to the *cis-trans* photoisomerization of AZ. The circular diagrams, however, did not suggest that reorientation of AZ influenced the relatively rich optical anisotropy observed in the π - π^* and n - π^* bands.

Figure 7 shows the polarized absorption spectra and circular diagrams for the π - π^* band at 318 nm and the n - π^* band at 440 nm of AZ and the d-d band at 603 nm for 2 in 2+laccase. An initial change in the π - π^* band was again observed due to *cis-trans* photoisomerization of AZ.

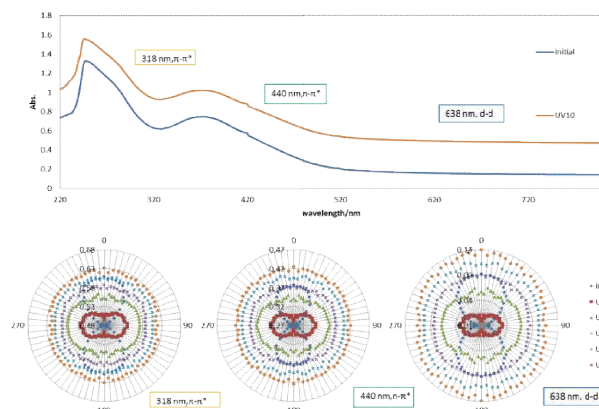


Figure 6. (Top) Polarized absorption spectra for 1+laccase at 0° showing predominant peaks before and after UV light irradiation for 10 min. (Bottom) Circular diagrams of the angular dependence of the absorbance of the predominant peaks in the polarized absorption spectra for 1+laccase after UV light irradiation for 0 (blue), 0.5 (red), 1 (green), 3 (violet), 5 (light blue), and 10 (orange) min.

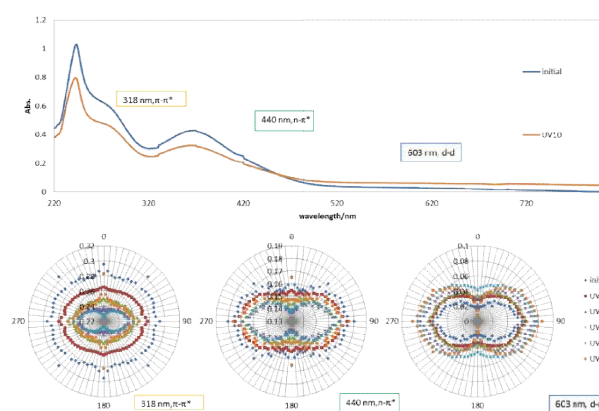


Figure 7. (Top) Polarized absorption spectra for 2+laccase at 0° showing predominant peaks before and after UV light irradiation for 10 min. (Bottom) Circular diagrams of the angular dependence of the absorbance of the predominant peaks in the polarized absorption spectra for 2+laccase after UV light irradiation for 0 (blue), 0.5 (red), 1 (green), 3 (violet), 5 (light blue), and 10 (orange) min.

Figure 8 shows the polarized absorption spectra and circular diagrams for the π - π^* band at 318 nm and the n - π^* band at 440 nm of AZ in 3+laccase.

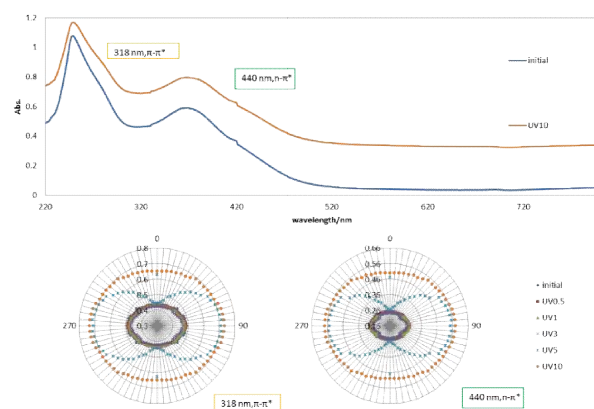


Figure 8. (Top) Polarized absorption spectra for 3+laccase at 0° showing predominant peaks before and after UV light irradiation for 10 min. (Bottom) Circular diagrams of the angular dependence of the absorbance of the predominant peaks in the polarized absorption spectra for 3+laccase after UV light irradiation for 0 (blue), 0.5 (red), 1 (green), 3 (violet), 5 (light blue), and 10 (orange) min.

3.4. Parameters for optical anisotropy.

Even for static molecules, the optical anisotropy of AZ and the complexes could be detected as changes in the absorption

intensity of the peaks in the polarized spectra because of changes in the direction of **AZ**. The Weigert effect also caused optical dichroism accompanied with photochemical reaction following polarized light irradiation. The molecular long axis of the reoriented *trans*-form of **AZ** became aligned in the direction perpendicular to the electric vector. The degree of photoinduced optical anisotropy of the polarized (electronic) spectra is commonly described using two parameters:

$$S = (A_{\text{parallel}} - A_{\text{perpendicular}}) / (2A_{\text{perpendicular}} + A_{\text{parallel}})$$

$$R = A_{\text{perpendicular}} / A_{\text{parallel}}$$

where $A_{\text{perpendicular}}$ and A_{parallel} denote the absorbance measured with polarizers perpendicular and parallel to the irradiated polarized light, respectively. For ideal isotropic systems, $S = 0$ and $R = 1$, and both the S and R parameters vary as the dichroism increases due to molecular alignment. A general treatment of *cis-trans* isomerization and the Weigert effect has been previously presented [25, 26]. The S and R values for the six materials investigated in the present study are summarized in Tables 1 and 2, respectively, and a qualitative discussion follows.

Table 1. R values determined from the polarized absorption spectra for **1+PMMA**, **2+PMMA**, and **3+PMMA** and **1+laccase**, **2+laccase**, and **3+laccase** after polarized UV light irradiation.

| UV irradiation (minutes) | initial | UV0.5 | UV1 | UV3 | UV5 | UV10 | |
|--------------------------|-----------------------------------|--------|---------|--------|--------|--------|--------|
| 1+PMMA | 318 nm, $\pi-\pi^*$ (AZ) | 1.0382 | 1.0100 | 1.0763 | 1.0328 | 1.0307 | 1.0202 |
| | 440 nm, $n-\pi^*$ (AZ) | 0.9471 | 0.8955 | 0.9205 | 0.8901 | 0.8874 | 0.8863 |
| | 612 nm, d-d (1) | 1.1813 | 1.0981 | 1.2469 | 1.1203 | 1.1341 | 1.1145 |
| 2+PMMA | 318 nm, $\pi-\pi^*$ (AZ) | 1.2030 | 1.4202 | 0.9729 | 0.9412 | 0.9217 | 0.9161 |
| | 440 nm, $n-\pi^*$ (AZ) | 1.1996 | 1.3915 | 0.9500 | 0.9112 | 0.8894 | 0.8772 |
| | 682 nm, d-d (2) | 2.0463 | 4.2954 | 0.9500 | 0.9816 | 0.9442 | 0.8841 |
| 3+PMMA | 318 nm, $\pi-\pi^*$ (AZ) | 1.0742 | 0.9848 | 0.9981 | 0.9825 | 1.0538 | 0.9851 |
| | 440 nm, $n-\pi^*$ (AZ) | 1.2023 | 1.2076 | 1.2167 | 1.1824 | 1.4752 | 1.1728 |
| | no d-d band | - | - | - | - | - | - |
| 1+laccase | 318 nm, $\pi-\pi^*$ (AZ) | 0.7194 | 0.9158 | 0.9628 | 0.9928 | 0.9940 | 1.0154 |
| | 440 nm, $n-\pi^*$ (AZ) | 0.5839 | 0.8503 | 0.9284 | 0.9732 | 0.9747 | 1.0079 |
| | 612 nm, d-d (1) | 5.2713 | -0.0243 | 0.8248 | 1.0728 | 1.0861 | 1.1959 |
| 2+laccase | 318 nm, $\pi-\pi^*$ (AZ) | 1.0049 | 0.9521 | 0.9377 | 0.9164 | 0.8731 | 1.0577 |
| | 440 nm, $n-\pi^*$ (AZ) | 0.9180 | 0.8846 | 0.8790 | 0.8250 | 0.8143 | 0.9332 |
| | 682 nm, d-d (2) | 0.3410 | 0.4556 | 0.5269 | 0.2923 | 0.5255 | 0.0970 |
| 3+laccase | 318 nm, $\pi-\pi^*$ (AZ) | 0.9058 | 0.8845 | 0.8864 | 0.9002 | 0.8857 | 0.8861 |
| | 440 nm, $n-\pi^*$ (AZ) | 0.9135 | 0.8694 | 0.8771 | 0.8916 | 0.8617 | 0.8629 |
| | no d-d band | - | - | - | - | - | - |

For the **PMMA** hybrid materials, the R values after irradiation for 10 min for the d-d bands of **1** and **2** were 1.1145 and 0.8841 for **1+PMMA** and **2+PMMA**, respectively. For the common $\pi-\pi^*$ bands of **AZ** near 318 nm, the R values after irradiation for 10 min were 1.0202, 0.9161, and 0.9851 for **1+PMMA**, **2+PMMA**, and **3+PMMA**, respectively.

For the laccase hybrid materials, the R values after irradiation for 10 min due to the d-d bands of **1** and **2** were 1.1959 and 0.0970 for **1+laccase** and **2+laccase**, respectively, and the R values for the common $\pi-\pi^*$ bands of **AZ** near 318 nm after

irradiation for 10 min were 1.0154, 1.0577, and 0.8861 for **1+laccase**, **2+laccase**, and **3+laccase**, respectively.

The results in Table 1 suggest that the degree of freedom may be determined by intermolecular interactions between the non-contact **AZ** molecules and **1**, **2**, or **3**. Identical behavior was observed for the S values summarized in Table 2.

Table 2. S values determined from the polarized absorption spectra for **1+PMMA**, **2+PMMA**, and **3+PMMA** and **1+laccase**, **2+laccase**, and **3+laccase** after polarized UV light irradiation.

| UV irradiation (minutes) | initial | UV0.5 | UV1 | UV3 | UV5 | UV10 | |
|--------------------------|-----------------------------------|--------|--------|--------|--------|--------|--------|
| 1+PMMA | 318 nm, $\pi-\pi^*$ (AZ) | 0.0126 | 0.0033 | 0.0248 | 0.0108 | 0.0101 | 0.0067 |
| | 440 nm, $n-\pi^*$ (AZ) | -0.017 | -0.036 | -0.027 | -0.038 | -0.039 | -0.039 |
| | 612 nm, d-d (1) | 9 | 1 | 2 | 0 | 0 | 4 |
| 2+PMMA | 318 nm, $\pi-\pi^*$ (AZ) | 0.0570 | 0.0317 | 0.0760 | 0.0386 | 0.0428 | 0.0368 |
| | 440 nm, $n-\pi^*$ (AZ) | 0.0634 | 0.1229 | -0.009 | -0.020 | -0.026 | -0.028 |
| | 682 nm, d-d (2) | 0.0624 | 0.1154 | -0.017 | -0.030 | -0.038 | -0.042 |
| 3+PMMA | 318 nm, $\pi-\pi^*$ (AZ) | 0.2586 | 0.5235 | -0.017 | -0.006 | -0.019 | -0.040 |
| | 440 nm, $n-\pi^*$ (AZ) | 0.0241 | -0.005 | -0.000 | -0.005 | 0.0176 | -0.005 |
| | no d-d band | 1 | 7 | 9 | 0 | 0 | 2 |
| 1+laccase | 318 nm, $\pi-\pi^*$ (AZ) | 0.0632 | 0.0647 | 0.0674 | 0.0573 | 0.1367 | 0.0545 |
| | 440 nm, $n-\pi^*$ (AZ) | - | - | - | - | - | - |
| | no d-d band | - | - | - | - | - | - |
| 2+laccase | 318 nm, $\pi-\pi^*$ (AZ) | -0.103 | -0.028 | -0.012 | -0.002 | -0.002 | 0.0051 |
| | 440 nm, $n-\pi^*$ (AZ) | 2 | 9 | 5 | 4 | 0 | 0 |
| | 612 nm, d-d (1) | -0.161 | -0.052 | -0.024 | -0.009 | -0.008 | 0.0026 |
| 3+laccase | 318 nm, $\pi-\pi^*$ (AZ) | 0 | 5 | 5 | 0 | 5 | 0.0026 |
| | 440 nm, $n-\pi^*$ (AZ) | -0.161 | -0.052 | -0.024 | -0.009 | -0.008 | 0.0026 |
| | no d-d band | 0 | 5 | 5 | 0 | 5 | 0.0026 |
| 1+laccase | 318 nm, $\pi-\pi^*$ (AZ) | 0.0016 | -0.016 | -0.021 | -0.028 | -0.044 | 0.0189 |
| | 440 nm, $n-\pi^*$ (AZ) | 2 | 2 | 7 | 2 | 2 | 0.0189 |
| | 682 nm, d-d (2) | -0.028 | -0.040 | -0.042 | -0.062 | -0.066 | -0.022 |
| 2+laccase | 318 nm, $\pi-\pi^*$ (AZ) | 1 | 0 | 0 | 0 | 0 | 8 |
| | 440 nm, $n-\pi^*$ (AZ) | -0.281 | -0.221 | -0.187 | -0.308 | -0.187 | -0.430 |
| | no d-d band | 5 | 7 | 2 | 7 | 9 | 6 |
| 3+laccase | 318 nm, $\pi-\pi^*$ (AZ) | -0.032 | -0.040 | -0.039 | -0.034 | -0.039 | -0.039 |
| | 440 nm, $n-\pi^*$ (AZ) | 4 | 1 | 4 | 4 | 6 | 5 |
| | no d-d band | -0.029 | -0.045 | -0.042 | -0.037 | -0.048 | -0.047 |
| 1+laccase | 318 nm, $\pi-\pi^*$ (AZ) | 7 | 5 | 7 | 5 | 3 | 9 |
| | 440 nm, $n-\pi^*$ (AZ) | 7 | 5 | 7 | 5 | 3 | 9 |
| | no d-d band | - | - | - | - | - | - |

Optical anisotropy depends not only on the flexibility of the coordination environment, but also on stable coordination geometries. The supramolecular chiral arrangement (such as chiral helical ordering) of **AZ** induced by the chiral complexes acting as chiral dopants and polarized UV light irradiation exhibiting the Weigert effect may therefore not result in any remarkable changes in the optical anisotropy parameters.

3.5. Analysis of the polarized spectra of the PMMA systems.

Metal ions that provide rigid coordination environments are known to be effective for increasing the molecular orientation resulting from the Weigert effect [40, 42-44]. In addition, the changes in the spectra of materials after linearly polarized UV light irradiation provide information on the molecular orientation and conformation and the coordination environment. Specifically, information regarding the molecular orientation and conformation can be obtained from the R and S values of the $\pi-\pi^*$ bands, while information regarding the coordination environment can be obtained from the R and S values of the d-d bands for the materials investigated in the present study. The data in Table 1 thus provided information regarding the molecular orientations and intermolecular interactions in these organic/inorganic hybrid materials. Notably, the initial change in the $\pi-\pi^*$ band intensity for **2+PMMA** was greater than that in the same bands for **1+PMMA** and **3+PMMA**. In fact, the order of the effect for the $\pi-\pi^*$ bands,

$n-\pi^*$ bands, and d-d bands was **2+PMMA >3+PMMA >1+PMMA**, **2+PMMA >1+PMMA >3+PMMA**, and **2+PMMA >1+PMMA**. These results indicate that the degree of increasing optical anisotropy accompanying the Weigert effect of **AZ** depended not only on the shapes of the chiral ligands, but also on the central nickel(II), copper(II), or zinc(II) ions. The circular diagrams also suggested an effective increase in the optical anisotropy for **2+PMMA**. This increase in the optical anisotropy for **2+PMMA** may be attributed to the molecular flexibility of copper(II) complexes. For **3+PMMA**, the increase in the optical anisotropy in the circular diagrams for the $\pi-\pi^*$ band may be attributed to the rigid tetrahedral coordination environment. In addition, the absence of a d-d band in the spectra for **3+PMMA** is a characteristic feature of zinc(II) complexes with a $3d^{10}$ electronic configuration [44].

Overall, the results demonstrate that differences in the nickel(II), copper(II), and zinc(II) ions in the analogous complexes are not limited to the behavior of the d-d bands, but can be detected as molecular flexibility [40, 45-49]. Such flexibility is reflected in the intermolecular interactions because of *cis-trans* photoisomerization and the molecular alignment of azo-containing ligands that result from the Weigert effect.

4. CONCLUSIONS

Organic/inorganic hybrid materials comprising azo-containing chiral Schiff base Ni(II), Cu(II), and Zn(II) complexes in **PMMA** or laccase matrices were prepared. Linearly polarized UV light irradiation resulted in an increase in the optical anisotropy of the materials, which was detected as changes in the $\pi-\pi^*$, $n-\pi^*$, and d-d bands in the polarized UV-Vis spectra (overlapped bands). The assignment and origin of the CD bands in the spectra of the hybrid materials containing chiral metal complexes and **AZ** after irradiation with polarized light was also discussed using TD-DFT calculations. For the **PMMA** films, the order of this effect was Cu(II) > Ni(II) > Zn(II). On the other hand, in the laccase films, the order of this effect was Zn(II) > Cu(II) >

5. REFERENCES

- [1] O. A. Blackburn, B. J. Coe, J. Fielden, M. Helliwell, J. J. W. McDounall, M. G. Hutchings, Nickel(II) and palladium(II) complexes of azobenzene-containing ligands as dichroic dyes, *Inorg. Chem.*, 49, 9136-9150, **2010**.
- [2] A. A. Khandar, Z. Revani, Preparation and thermal properties of the bis[5-((4-heptyloxyphenyl)azo)-N-(4-alkoxyphenyl)-salicylaldiminato]copper(II) complex homologues *fn1*, *Polyhedron*, 18, 129-133, **1998**.
- [3] Y. Einaga, M. Taguchi, G. Li, T. Akitsu, T. Sugai, O. Sato, Magnetization Increase of Iron Oxide by the Photo-Induced Aggregation of Spiropyran, *Chem. Mater.*, 15, 8-10, **2003**.
- [4] R. Mikami, M. Taguchi, K. Yamada, K. Suzuki, O. Sato, Y. Einaga, Reversible Photo-Switching of the Magnetization of Iron Oxide Nanoparticles at Room Temperature, *Angew. Chem. Int. Ed.*, 43, 6135-6139, **2004**.
- [5] M. Taguchi, K. Yamada, K. Suzuki, O. Sato, Y. Einaga, Photo-switchable Magnetic Nanoparticles of Prussian Blue with Amphiphilic Azobenzene, *Chem. Mater.*, 17, 4554-4559, **2005**.
- [6] T. Yamamoto, Y. Umemura, O. Sato, Y. Einaga, Observation of the Anisotropic Photoinduced Magnetization Effect in Co-Fe Prussian Blue Thin Films Fabricated by Using the Clay Langmuir-Blodgett Films as a Template, *J. Am. Chem. Soc.*, 127, 16065-16073, **2005**.
- [7] T. Yamamoto, Y. Umemura, O. Sato, Y. Einaga, Photoswitchable Magnetic Films: Prussian Blue Intercalated in Langmuir-Blodgett Films

3.6. Analysis of the polarized spectra of the laccase systems.

As with the PMMA systems, the R and S values for the laccase systems provide information on the molecular orientation and conformation and the coordination environment. Thus, using the data in Table 1, information regarding the molecular orientations and intermolecular interactions in the laccase systems was derived. Notably, the initial change in the $\pi-\pi^*$ band intensity for **1+laccase** was greater than that in the same bands for **2+laccase** and **3+laccase**. The order of the effect for the $\pi-\pi^*$ bands, $n-\pi^*$ bands, and d-d bands was **3+laccase > 2+laccase > 1+laccase**, **3+laccase > 2+laccase > 1+laccase**, and **2+laccase > 1+laccase**, respectively. In particular, the increase in the optical anisotropy of the d-d band for **2+laccase** is quite remarkable. In general, the results of the optical anisotropy analysis of the laccase systems can be summarized and discussed similarly to those for the PMMA systems.

There were remarkable differences due to the different matrices. However, in the laccase films, increasing the optical anisotropy in the rigid nickel(II) complex was easier than in the flexible copper(II) complex, as reflected in both the $n-\pi^*$ and $\pi-\pi^*$ bands. Thus, the differences in the optical anisotropy of the laccase and PMMA films may be attributed to both the greater flexibility of the PMMA and the chirality of the laccase.

Ni(II). These results suggested that the differences in optical anisotropy can be ascribed to intermolecular interactions between the azo-groups due to the flexibility of the coordination environment of the metal centers of the complexes. In addition, in the **PMMA** films, the optical anisotropy of the $n-\pi^*$ band and $\pi-\pi^*$ bands increased more easily for the copper(II) complex than the nickel(II) complex. In the laccase films, in contrast, the optical anisotropy of the $n-\pi^*$ band and $\pi-\pi^*$ bands increased more readily for the rigid nickel(II) complex than the flexible copper(II) complex. These results suggested that the differences in optical anisotropy were also in part due to the flexibility of the matrix.

- Consisting of an Amphiphilic Azobenzene and a Clay Mineral, *Chem. Mater.*, 16, 1195-1201, **2004**.
- [8] Y. Einaga, R. Mikami, T. Akitsu, G. Li, Reversible photocontrol of molecular assemblies of metal complex containing azo-amphiphiles, *Thin Solid Films*, 493, 230-236, **2005**.
- [9] T. Akitsu, A. Yoshida, Detection of Intermolecular Interaction Between Pd(II) Complexes Having Imidate and Amine Ligands and Photochromic Dyes in Hybrid Solution Systems by Absorption and Fluorescence Spectra, *Curr. Phys. Chem.*, 1, 76-81, **2011**.
- [10] T. Akitsu, S. Yamamoto, Spectroscopic detection of photofunctional systems of copper(II) complexes, Azo-dye, and TiO₂, *Asian Chem. Lett.*, 14, 255-260, **2010**.
- [11] T. Akitsu, Y. Einaga, Synthesis, crystal structures, and electronic properties of Schiff base nickel(II) complexes: Towards solvatochromism induced by photochromic solute, *Polyhedron*, 24, 1869-1877, **2005**.
- [12] T. Akitsu, Y. Einaga, Syntheses, crystal structures, and electronic properties of a series of copper(II) complexes with 3,5-halogen-substituted Schiff base ligands and their solutions, *Polyhedron*, 24, 2933-2943, **2005**.
- [13] T. Akitsu, Photofunctional supramolecular solution systems of chiral Schiff base nickel(II), copper(II), and zinc(II) complexes and photochromic azobenzenes, *Polyhedron*, 26, 2527-2535, **2007**.

- [14] T. Akitsu, Y. Einaga, Novel photo-induced aggregation behavior of a supramolecular system containing iron(III) magnetic ionic liquid and azobenzene, *Inorg. Chem. Commun.*, 9, 1108-1110, **2006**.
- [15] T. Akitsu, J. Nishijo, The first detection of photomodulation by both DC and in-phase AC susceptibility for organic/inorganic hybrid materials containing cyano-bridged Gd-Cr complex and azobenzene, *J. Magn. Magn. Matter.*, 320, 1586-1590, **2008**.
- [16] T. Akitsu, J. Nishijo, The first observation of photoinduced tuning of AC magnetization for organic/inorganic hybrid materials composed of Mn₁₂-acetate and azobenzene, *J. Magn. Magn. Matter.*, 315, 95-100, **2007**.
- [17] T. Akitsu, The tuning of quantum magnetization for organic/inorganic hybrid materials composed of Mn₁₂-acetate and azobenzene casted into PMMA films on PVA films, *J. Magn. Magn. Matter.*, 321, 207-212, **2008**.
- [18] E. I. Solomon, R. K. Szilagy, S. D. George, L. Basumallick, Electronic structures of metal sites in proteins and models: contributions to function in blue copper proteins, *Chem. Rev.*, 104, 419-458, **2004**.
- [19] E. I. Solomon, M. J. Badwin, M. D. Lowery, Electronic Structures of Active Sites in Copper Proteins: Contributions to Reactivity, *Chem. Rev.*, 92, 521-542, **1992**.
- [20] G. Weber, Polarization of the fluorescence of macromolecules. 1. Theory and experimental method, *Biochem. J.*, 51, 145-155, **1952**.
- [21] G. Weber, Polarization of the fluorescence of macromolecules. 2. Fluorescent conjugates of ovalbumin and bovine serum albumin, *Biochem. J.*, 51, 155-167, **1952**.
- [22] D. M. Jameson, J. A. Ross, Fluorescence polarization/anisotropy in diagnostics and imaging, *Chem. Rev.*, 110, 2685-2708, **2010**.
- [23] M. R. Hicks, J. Kowalski, A. Rodger, LD spectroscopy of natural and synthetic biomaterials, *Chem. Soc. Rev.*, 39, 3380-3393, **2010**.
- [24] G. Pescitelli, L. D. Bari, N. Berova, Conformational aspects in the studies of organic compounds by electronic circular dichroism, *Chem. Soc. Rev.*, 40, 4603-4625, **2011**.
- [25] F. Weigert, Uebereineneuen Effect der Strahlung, *Naturwissenschaften*, 29, 583-589, **1921**.
- [26] K. Ichimura, Photoalignment of Liquid-Crystal Systems, *Chem. Rev.*, 100, 1847-1874, **2000**.
- [27] T. Akitsu, C. Ishioka, Manipulation and Observation by Polarized Light: Hybrid Materials of Chiral Schiff Base Mn(III) Complexes and Azobenzene in PMMA, *Asian Chem. Lett.*, 14, 37-51, **2010**.
- [28] T. Akitsu, T. Itoh, Polarized spectroscopy of hybrid materials of chiral Schiff base cobalt(II), nickel(II), copper(II), and zinc(II) complexes and photochromic azobenzenes in PMMA films, *Polyhedron*, 29, 477-487, **2010**.
- [29] T. Akitsu, C. Ishioka, T. Itoh, Polarized Spectroscopy of Hybrid Materials of Mn₁₂ Single-Molecule Magnet and Azobenzene or Disperse Red 1 in PMMA Films, *Cent. Eur. J. Chem.*, 7, 690-696, **2009**.
- [30] T. Akitsu, R. Tanaka, Polarized Electronic and IR Spectra of Hybrid Materials of Chiral Mn(II) Complexes and Different Types of Photochromic Dyes Showing Photoisomerization or Weigert Effect, *Curr. Phys. Chem.*, 1, 82-89, **2011**.
- [31] T. Akitsu, Y. Miura, Polarized electronic spectra of organic/inorganic hybrid materials of chiral Schiff base Ni(II) or Cu(II) complexes and disperse red 1 or azobenzene in PMMA films, *J. Chem. Chem. Eng.*, 5, 443-450, **2011**.
- [32] Y. Aritake, T. Takanashi, A. Yamazaki, T. Akitsu, Polarized spectroscopy and hybrid materials of chiral Schiff base Ni(II), Cu(II), Zn(II) complexes with included or separated azo-groups, *Polyhedron*, 30, 886-894, **2011**.
- [33] T. Akitsu, R. Tanaka, Polarized Electronic and IR Spectroscopy of Hybrid Materials of Chiral Cu(II) and Mn₁₂ Complexes and Some Photochromic Compounds in PMMA Films, *Asian Chem. Lett.*, 14, 235-254, **2010**.
- [34] M. Ito, T. Akitsu, Polarized UV light induced molecular arrangement depending on flexibility of chiral Schiff base Ni(II), Cu(II), and Zn(II) complexes by azobenzene in PMMA matrix, *Contemp. Eng. Sci.*, 7, 869-877, **2014**.
- [35] Y. Aritake, T. Akitsu, The role of chiral dopants in organic/inorganic hybrid materials containing chiral Schiff base Ni(II), Cu(II), and Zn(II) complexes, *Polyhedron*, 31, 278-584, **2012**.
- [36] A. Yamazaki, T. Akitsu, Polarized spectroscopy and polarized UV light-induced molecular orientation of chiral diphenyl Schiff base Ni(II) and Cu(II) complexes and azobenzene in a PMMA film, *RSC Adv.*, 2, 2975-2980, **2012**.
- [37] Y. Tan, W. Deng, Y. Li, Z. Huang, Y. Meng, Q. Xie, M. Ma, S. Yao, Polymeric bionanocomposite cast thin films with in situ laccase-catalyzed polymerization of dopamine for biosensing and biofuel cell applications, *J. Phys. Chem. B.*, 114, 5016-5024, **2010**.
- [38] N. Hariu, M. Ito, T. Akitsu, Linearly, Circularly, or Non-polarized Light Induced Supramolecular Arrangement of Diastereomer Schiff Base Ni(II), Cu(II), and Zn(II) Complexes by Azobenzene in PMMA Matrix, *Contemp. Eng. Sci.*, 8, 57-70, **2015**.
- [39] Y. Aritake, Y. Watanabe, T. Akitsu, Chiral photochromic Schiff base: 4-phenylazo-2-[[[(R)-(1-phenylethyl)imino]methyl]phenol], *Acta Cryst.*, E66, o749-o749, **2010**.
- [40] M. J. Frisch, G. W. Trucks, H. B. Schlegel, G. E. Scuseria, M. A. Robb, J. R. Cheeseman, G. Scalmani, V. Barone, B. Mennucci, G. A. Petersson, H. Nakatsuji, M. Caricato, X. Li, H. P. Hratchian, A. F. Izmaylov, J. Bloino, G. Zheng, J. L. Sonnenberg, M. Hada, M. Ehara, K. Toyota, R. Fukuda, J. Hasegawa, M. Ishida, T. Nakajima, Y. Honda, O. Kitao, H. Nakai, T. Vreven, J. A. Montgomery, Jr., J. E. Peralta, F. Ogliaro, M. Bearpark, J. J. Heyd, E. Brothers, K. N. Kudin, V. N. Staroverov, R. Kobayashi, J. Normand, K. Raghavachari, A. Rendell, J. C. Burant, S. S. Iyengar, J. Tomasi, M. Cossi, N. Rega, J. M. Millam, M. Klene, J. E. Knox, J. B. Cross, V. Bakken, C. Adamo, J. Jaramillo, R. Gomperts, R. E. Stratmann, O. Yazyev, A. J. Austin, R. Cammi, C. Pomelli, J. W. Ochterski, R. L. Martin, K. Morokuma, V. G. Zakrzewski, G. A. Voth, P. Salvador, J. J. Dannenberg, S. Dapprich, A. D. Daniels, O. Farkas, J. B. Foresman, J. V. Ortiz, J. Cioslowski, and D. J. Fox, Gaussian, Inc., Wallingford CT, **2009**.
- [41] S. Yamada, Advancement in stereochemical aspects of Schiff base metal complexes, *Coord. Chem. Rev.*, 190-192, 537-555, **1999**.
- [42] T. Akitsu, Y. Einaga, Bis[(R)-3,5-dichloro-N-(1-phenylethyl)salicylideneamino-κ₂N,O]copper(II) and
- [43] Bis[(R)-3-ethoxy-N-(1-phenylethyl)salicylideneamino-κ₂N,O]copper(II), *Acta Cryst.*, C60, m640-m642, **2004**.
- [44] T. Akitsu, Y. Einaga, Synthesis and crystal structures of flexible Schiff base complex, bis(N-1,2-diphenylethyl-salicydenamino-κ²N,O)copper(II) (methanol): a rare case of solvent-induced distortion, *Polyhedron*, 25, 1089-1095, **2006**.
- [45] C. Evans, D. Luneau, New Schiff base zinc(II) complexes exhibiting second harmonic generation, *J. Chem. Soc., Dalton Trans.*, 83-86, **2002**.
- [46] H. Sakiyama, H. Okawa, N. Matsumoto, S. Kida, A Tetrahedral Zinc(II) Complex of N-(R)-1-Phenylethylsalicylaldimine. Structural and Circular Dichroism Spectral Investigation on Stereoselectivity, *J. Chem. Soc., Dalton Trans.*, 2935-2939, **1990**.
- [47] B. Bosnich, An interpretation of the circular dichroism and electronic spectra of salicylaldimine complexes of square-coplanar diamagnetic nickel(II), *J. Am. Chem. Soc.*, 90, 627-632, **1968**.
- [48] H. Okawa, M. Nakamura, S. Kida, Noncovalent interactions in metal complexes. 12. Stereoselectivity of tetrahedral or pseudotetrahedral bis(N-1-menthyl-salicylaldiminato)M(II) and bis(N-1-menthyl-3-methylsalicylaldiminato)M(II) (M = Co, Cu, Ni, Zn), *Inorg. Chim. Acta*, 120, 185-189, **1986**.
- [49] Y. Nishida, S. Kida, A Study of Electronic Spectra of Square Planar Copper(II) and Nickel(II) Complexes by Circular Dichroism, *Bull. Chem. Soc. Jpn.*, 43, 3814-3819, **1970**.
- [50] H. Sakiyama, H. Okawa, N. Matsumoto, S. Kida, Stereoselectivity in Diastereomeric Tetrahedral Metal(II) Complexes of Chiral Salicylideneamines: Crystal Structure and Molecular Mechanics Calculation of Bis[N-(1-menthyl)salicylideneamino]cobalt(II), *Bull. Chem. Soc. Jpn.*, 64, 2644-2647, **1991**.
- [51] M. Ulusoy, H. Karabiyik, R. Kilincarslan, M. Aygun, B. Cetinkaya, S. Garcia-Granda, Co(II) and Cu(II) Schiff base complexes of bis(N-(4-diethylamino-2-methylphenyl)-3,5-di-tert-butylsalicylaldimine): Electrochemical and X-ray structural study, *Struct. Chem.*, 19, 749-755, **2008**.

6. ACKNOWLEDGEMENTS

This work was supported by the Research Foundation for Opto-Science and Technology. The computations were performed at the Research Centre for Computational Science, Okazaki, Japan.

© 2015 by the authors. This article is an open access article distributed under the terms and conditions of the Creative Commons Attribution license (<http://creativecommons.org/licenses/by/4.0/>).